GEOPHYSICS, VOL. 50, NO. 4 (APRIL 1985); P. 656–664, 14 FIGS.

Geophysical exploration with audiofrequency natural magnetic fields

V. F. Labson*, A. Becker‡, H. F. Morrison‡, and U. Conti‡

ABSTRACT

Experience with the AFMAG method has demonstrated that an electromagnetic exploration system using the Earth's natural audiofrequency magnetic fields as an energy source is capable of mapping subsurface electrical structure in the upper kilometer of the Earth's crust. We resolved the limitations of this method by adapting the tensor analysis and remote reference noise bias removal techniques from the geomagnetic induction and magnetotelluric methods to computation of the tippers.

After a thorough spectral study of the natural magnetic fields, we designed lightweight magnetic field sensors capable of measuring the magnetic field throughout the year. We also built a digital acquisition and processing system with the ability to provide audiofrequency tipper results in the field.

This new instrumentation was used in a study of the Mariposa, California site previously mapped with AFMAG. This study once again demonstrates the usefulness of natural magnetic field data in mapping an electrically conductive body. Reoccupation of one of the sites in several different seasons proves the high level of repeatability of these data. As well as being repeatable, the tensor data provide additional information on the geometry of the conductive body. Different electrical conductivity features can be distinguished using a broad band of frequencies.

INTRODUCTION

The Audio Frequency MAGnetic (AFMAG) technique (Ward, 1959) was proposed as an efficient method for mapping the subsurface electrical conductivity structure; however, AFMAG suffers from several severe limitations (Ward et al., 1966) which have prevented its widespread application.

AFMAG's limitations may be removed by use of signal processing and data aquisition techniques developed for two closely related geophysical methods. The source fields for both AFMAG and our revision are natural electromagnetic (EM) fields in the 1 Hz to 20 kHz band associated with lightning discharges in the Earth-ionosphere cavity. At some distance from the source, these fields propagate as plane waves with a vertical electric field E_z and a horizontal transverse magnetic field H that is perpendicular to the direction of propagation. Because of finite ground conductivity, the propagating wave is tilted slightly in the direction of propagation to accommodate a horizontal electric field E_r at the Earth-air interface. In most areas the Earth is sufficiently conductive that its surface impedance E_r/H is the same as that for a plane wave normally incident to the surface. In areas where the ground is homogeneous, this description of the propagating EM field is complete. The presence of lateral conductivity variations gives rise to a vertical magnetic field component related to the distortion in the subsurface current pattern. In the simplest case, where the incident wave propagates along the strike direction of a two-dimensional (2-D) inhomogeneity, the normally horizontal transverse magnetic field vector in the vicinity of the anomalous feature may be sharply rotated toward vertical.

Generation of vertical magnetic fields by subsurface inhomogeneities is not limited to the audiofrequency band. The same phenomenon occurs with inducing fields originating in the ionosphere and magnetosphere. The spectrum for these fields extends from below 10^{-4} up to 1 Hz. Studies of the vertical magnetic field at the low frequencies as a means of investigating conductive anomalies in the deep crust and upper mantle are called the geomagnetic induction method. The history and development of this geophysical technique were excellently summarized by Schmucker (1970). The vertical field has also been included in the studies of the surface tensor impedance (magnetotellurics, MT). In magnetotellurics a coefficient called the tipper relates the vertical to the horizontal magnetic fields. A good review of the use of the tipper in geologic studies was presented in Vozoff (1972). Our studies of tipper profile data show that in a number of geologically simple cases they can be uniquely interpreted in terms of the subsurface electrical structure.

Weak fields and inadequate equipment have prevented widespread application of tensor magnetotellurics in the audiofrequency band which is appropriate for exploration and geologic mapping in the upper kilometer of the crust. Bostick et al. (1977) documented the development of such a system, but their ability to make successful tipper measurements has not been reported. Several studies of scalar audio magnetotellurics have

Manuscript received by the Editor May 21, 1984; revised manuscript received October 19, 1984.
*Engineering Geoscience, University of California, Berkeley, CA; also U.S. Geological Survey, Denver, CO.
‡Engineering Geoscience, Hearst Mining Building, University of California, Berkeley, CA 94720.
This paper was prepared by an agency of the U.S. government.

appeared in the literature (Strangway et al., 1973; Hoover et al., 1978), but these did not incorporate tipper measurements.

AFMAG, a simple method for indicating and mapping near-surface conductive features by measuring the tilt of the magnetic field, was first reported by Ward (1959). This method uses two orthogonal coils to sense the audiofrequency magnetic fields. The coils, tuned typically to 150 and 500 Hz, are first oriented with their axes in the horizontal plane, so one of them lies in the direction of the principal horizontal magnetic field component. They are then rotated into the vertical plane passing through this azimuth, and the dip of the major axis of the polarization ellipse is determined. The polarization direction of the horizontal magnetic field depends upon the worldwide distribution of lightning which varies with time, and in fact has a distinct seasonal variation. The AFMAG results also vary with time because the induction process and the resulting vertical magnetic field change as the orientation of the inducing field is altered. In spite of this fundamental shortcoming, the AFMAG method was used successfully in several reconnaissance exploration projects such as those described in Ward et al. (1966).

An equally serious problem with AFMAG is the fact that the signal strength is inadequate in high latitudes in the winter. The inherent noise level of the coils and their electronics is higher than the level of the weak signals originating in storms at the equator and southern temperate zones. Finally, the ability of AFMAG to distinguish between near-surface and deep features was severely limited because only two frequencies were used for interpretation.

Because of the great potential for a geophysical method based on a broadband quantitative analysis of the natural audiofrequency electromagnetic spectrum, we decided to revise the AFMAG method. We incorporated a more rigorous approach to the measurement and analysis of the fields using some of the techniques developed for geomagnetic induction and magnetotellurics, and we investigated new sensors that are effective in low signal conditions.

FIELD THEORY

In geomagnetic induction and magnetotellurics the vertical magnetic field is related to the horizontal magnetic field through a transfer tensor, the tipper $\mathbf{T}$ defined (Vozoff, 1972) by

$$H_z(\omega) = T_x(\omega)H_x(\omega) + T_y(\omega)H_y(\omega). \tag{1}$$

The tipper is complex and a function of frequency. While T_x and T_y are dependent upon the measurement coordinate system, $\mathbf{T}$'s magnitude and direction are rotationally invariant functions of subsurface electrical conductivity distribution and do not depend upon the polarization of the inducing field. In AFMAG a quantity proportional to some T_x was used where the x-direction was taken along the average principal direction of the horizontal magnetic field. Since this direction changed with time, the scalar T_x for a 2-D case could vary from zero to the maximum determined by the tensor form given above.

In equation (1), $H_z(\omega)$, $H_x(\omega)$, and $H_y(\omega)$ are the Fourier transforms of the time-varying magnetic field. If this equation were first multiplied through by the complex conjugate of $H_x(\omega)$ and then again by the complex conjugate of $H_y(\omega)$ and if the results were averaged over many data sets, we would obtain the following two simultaneous equations:

$$\langle H_z H_x^* \rangle = T_x \langle H_x H_x^* \rangle + T_y \langle H_y H_x^* \rangle, \tag{2}$$

and

$$\langle H_z H_y^* \rangle = T_x \langle H_x H_y^* \rangle + T_y \langle H_y H_y^* \rangle. \tag{3}$$

Time averages are denoted by $\langle\ \rangle$ and the dependence on ω is omitted from the notation. These two equations in the auto- and cross-powers of the magnetic field components can be solved for the tipper components T_x and T_y

$$T_x = \frac{\langle H_z H_x^* \rangle \langle H_y H_y^* \rangle - \langle H_z H_y^* \rangle \langle H_y H_x^* \rangle}{\langle H_x H_x^* \rangle \langle H_y H_y^* \rangle - \langle H_y H_x^* \rangle \langle H_x H_y^* \rangle}, \tag{4}$$

and

$$T_y = \frac{\langle H_z H_y^* \rangle \langle H_x H_x^* \rangle - \langle H_z H_x^* \rangle \langle H_x H_y^* \rangle}{\langle H_x H_x^* \rangle \langle H_y H_y^* \rangle - \langle H_y H_x^* \rangle \langle H_x H_y^* \rangle}. \tag{5}$$

Using H_x and H_y to obtain equations (4) and (5) has been traditional in magnetotellurics, but for the estimates of T_x and T_y to be unbiased, H_x and H_y must be noise free. If noise (for example, noise in the sensor) is present, then the auto-power terms will contain a noise component that will add to the signal power no matter how much averaging is used.

This problem may be solved if only cross-spectral estimates are used (Anav et al., 1976; Bendat and Piersol, 1971). Suppose that another field $\mathbf{R}$, coherent with H_x and H_y, is measured; it is assumed that the noise accompanying this field is independent of the noise in H_x and H_y. The expected value of $\langle H_x R_x^* \rangle$, $E\langle H_x R_x^* \rangle$ can be expanded and written as

$$E\langle H_x R_x^* \rangle = E\langle (H_x + n_x)(R_x^* + n_r^*) \rangle, \tag{6}$$

where n_x and n_r are the noises present in H_x and R_x, respectively. Since $E\langle H_x n_r^* \rangle$, $E\langle R_x^* n_x \rangle$, and $E\langle n_x n_r^* \rangle$ are all zero, the expected value of $\langle H_x R_x^* \rangle$ is unbiased. Using R_x^* and R_y^*, equations (4) and (5) become

$$T_x = \frac{\langle H_z R_x^* \rangle \langle H_y R_y^* \rangle - \langle H_z R_y^* \rangle \langle H_y R_x^* \rangle}{\langle H_x R_x^* \rangle \langle H_y R_y^* \rangle - \langle H_y R_x^* \rangle \langle H_x R_y^* \rangle}, \tag{7}$$

and

$$T_y = \frac{\langle H_z R_y^* \rangle \langle H_x R_x^* \rangle - \langle H_z R_x^* \rangle \langle H_x R_y^* \rangle}{\langle H_x R_x^* \rangle \langle H_y R_y^* \rangle - \langle H_y R_x^* \rangle \langle H_x R_y^* \rangle}. \tag{8}$$

T_x and T_y determined in this fashion are free of noise bias (Gamble et al., 1979a). In practice the reference fields may be obtained from separate measurements of the magnetic fields from sensors some distance away, or from measurements of the associated electric fields. This method of eliminating the auto-spectral noise can be used to obtain unbiased tipper estimates at virtually any signal level, given sufficient averaging time. It can also be used to obtain accurate measurements of the natural field spectrum and the noise spectra of the sensors.

NATURAL MAGNETIC FIELD SPECTRUM

Successful implementation of the referenced tipper method required that the major advantages of AFMAG—speed of operation and portability—be retained. To accomplish this, we had to design new lightweight magnetic field sensors; we undertook to study the natural magnetic field spectrum to determine the signal level which these sensors would be required to detect. Previous spectral studies of Hoover et al. (1978), Maxwell and

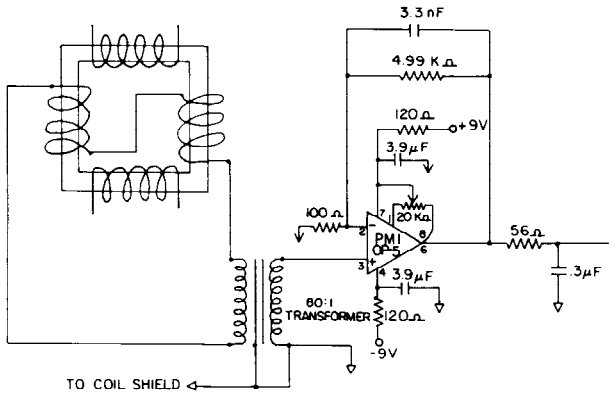

FIG. 1. U.S.G.S. two-component induction coil (only one amplifier shown).

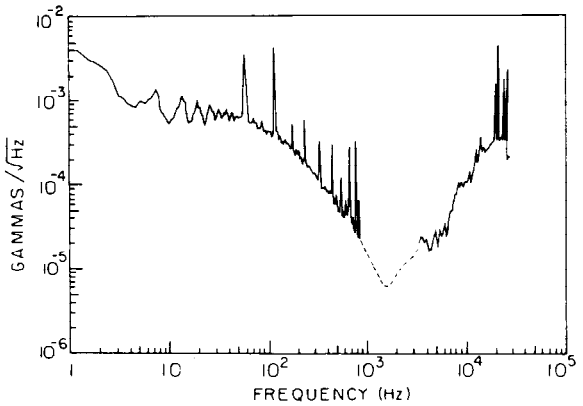

FIG. 2. Typical summer spectrum at San Antonio Valley, California, July 14, 1980.

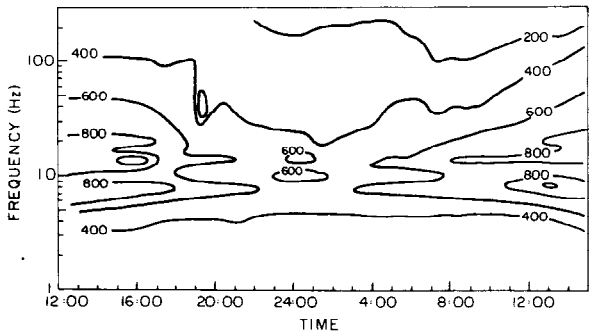

FIG. 3. Sonogram of natural field spectrum at San Antonio Valley, California, August 27–28, 1979; contours in $\mu\gamma/\sqrt{\text{Hz}}$.

Stone (1963), and Telford (1977) showed the extreme variability of spectral signal levels. This new study was designed to verify the previous results and to demonstrate the effectiveness of the cross-spectral technique for determining the spectra of audio-frequency magnetic fields.

Spectra determinations were made initially using sets of induction coil sensors loaned to the University of California by Kennecott Copper Corp. and the U.S. Geological Survey (U.S.G.S.). Both sensors have a response proportional to the time derivative of the magnetic field. The U.S.G.S. two-component sensor is composed of a square Ceramic Magnetics[1] MN-60 ferrite frame 0.36 m on a side with a rectangular cross-section of 3.8×10^{-2} m by 1.8×10^{-2} m. Each leg is wound in two layers with 186 turns of no. 14 copper wire. Parallel legs are connected in series and coupled to a low-noise amplifier by an 80 : 1 iron-cored transformer (Figure 1). The cross talk between the two orthogonal components of this sensor is less than −40 dB. The coil-transformer has a sensitivity of 2.3×10^{-5} V/(nT Hz) and a self-resonant frequency of 1.3 kHz. The packaged sensor is enclosed in a metallic foil electrostatic shield and weighs 13.4 kg. This coil has been in field use making scalar audiomagnetotelluric measurements for several years (Hoover et al., 1978). Although no technical details were available for the Kennecott coils, their sensitivity was found to be 8.3×10^{-6} V/(nT Hz).

The spectral measurements were made at San Antonio Valley, California, approximately 48 km southeast of Livermore, California. This site was selected for its low cultural noise level and its convenience. The 60 Hz power line noise and the associated harmonics from a power line approximately 4 km away are the major noise constituents at this site. The 60 Hz noise is of the order of 10^{-2} nT_{rms}.

To obtain the required spectra, the outputs from a pair of sensors were first amplified and filtered and then digitally processed by a Hewlett-Packard 3582A spectrum analyzer. The spectra (computed by a 512 point fast Fourier transform) were directly transferred to an on-line Hewlett-Packard 9825S computer that corrected the spectra to magnetic field units. All spectral measurements were made over a broad band of frequencies using an averaging time of 2 minutes. The results were displayed in the field using a digital plotter linked to the computer. A motor-generator set provided 120 Vac power, but it created some additional noise.

Figure 2 shows a typical spectrum recorded in the early afternoon in the summer season. The dominant features are the Schumann resonances at 8, 14, and 20 Hz; the 60 Hz powerline and motor generator noise with its harmonics; and the VLF radio stations from 17 to 25 kHz. The spectrum shows a distinct minimum between 1 and 2 kHz. Here the spectral amplitudes shown are approximate, since we could not determine these field levels to the same degree of accuracy as the rest of the spectrum.

Over a 24 hour period the field levels peak in the early afternoon and decrease into the very early morning hours (Figure 3). A yearly variation is also seen with the peak level in mid to late summer and a minimum in the winter (Figure 4).

COIL DEVELOPMENT

Design principles

Based on the spectral studies, a lightweight mu-metal cored sensor was designed and built at the University of California, on a design resembling that described by MacIntyre (1980) for an air-core coil. In order to obtain a constant sensitivity over a

[1]Any use of trade names is for descriptive purposes only and does not imply endorsement by the U.S. Geological Survey.

large band of frequencies and close correspondence in amplitude and phase characteristics between different sensors, we detect the current in the induction coil by using a current-to-voltage amplifier (Figure 5).

The coil is composed of 45 000 turns of no. 31 copper wire with a resistance of 2 000 Ω wound on a 0.6 m long by 0.016 m diameter laminated mu-metal core. The coil has an inductance of 500 H and is enclosed in a metallic foil electrostatic shield. A small capacitor is wired in parallel to the innermost 6 000 turns to reduce secondary resonances. The coil-amplifier combination is 0.62 m long and 0.06 m in diameter and weighs 2.5 kg. The resulting sensor has a sensitivity of 0.05 V/nT in the audiofrequency range. At frequencies below 0.2 Hz, the sensor has a response proportional to frequency. This coil is quite stable even in the presence of large magnetic field impulses. Different coils of this design match in amplitude and phase sensitivity to within 1 percent. This coil was also quite adequate for making the cross-spectral measurements. The sensitivity function for the UC detector is compared to that of the U.S.G.S. coil with amplifier in Figure 6. There is no need for a phase correction below 500 Hz. This is a considerable advantage for the relatively slow field computer.

Noise measurements

Coil noise spectra were determined in three ways: (1) in-field cross-spectral technique, (2) in a mu-metal shield, and (3) numerical simulation on the computer. The three methods yielded similar results.

The in-field cross-spectral technique determines the coil noise by comparison of the noise-free cross-spectral estimate of equation (6) and the sum of signal and noise represented by the auto-spectral estimate, assuming that the natural field is uniform over the 3 m coil separation and that the coil noises are independent. Thus,

$$\langle H_x H_x^* \rangle - \langle R_x H_x^* \rangle = \langle n_x n_x^* \rangle. \tag{9}$$

Tests using the mu-metal shield at the U.S. Geological Survey's Denver laboratory provided an independent measurement of the coil noise. The level of coherence at frequencies above 1 Hz between a coil placed in the shield and one outside a short distance away was measurable only at 20 Hz and 60 Hz and its harmonics.

In the absence of an external field the output of a coil is the internal noise of that coil. In a highly shielded environment such as that in the mu-metal shield, the output must be greater than or equal to the internal noise. This measurement gives a baseline for comparison with the noise determined from the cross-spectral technique, provided that the noise is not field-strength dependent. The agreement with the cross-spectral noise measurements made at various field levels indicates that the noise is not field-strength dependent.

The coil's noise was also computed numerically using SPICE, a general purpose circuit simulation program developed by the Dept. of Electrical Engineering and Computer Science at the University of California (Vladimirescu et al., 1981). The results were used in the coil design and in verification of the experimental noise determinations.

The numerical model considered both the Johnson noise of the resistive elements and the amplifier noise. The resistive noise power is determined by

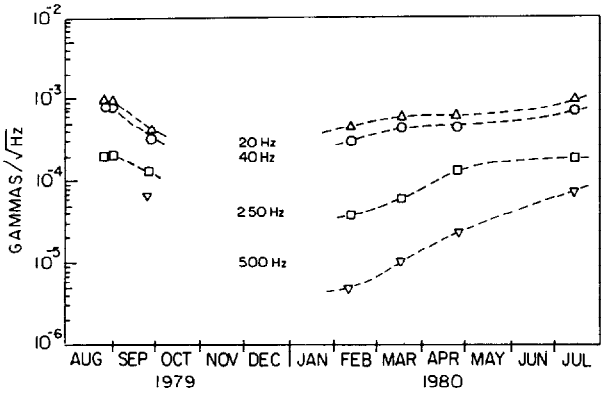

FIG. 4. Annual spectral variation at San Antonio Valley, California.

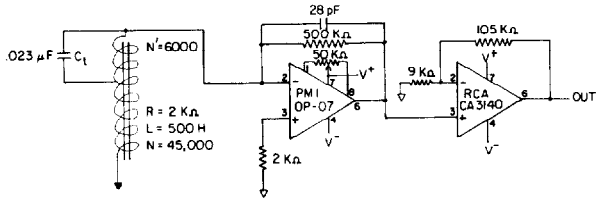

FIG. 5. University of California induction coil magnetometer.

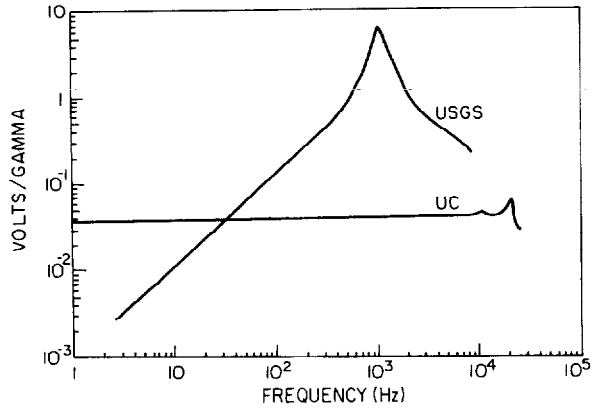

FIG. 6. Amplitude response of U.S.G.S. and University of California coils.

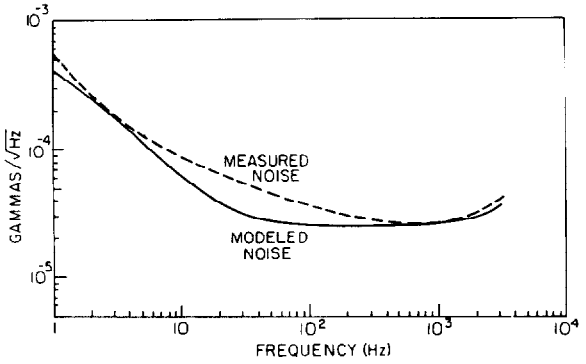

FIG. 7. Measured and modeled noise of University of California coil.

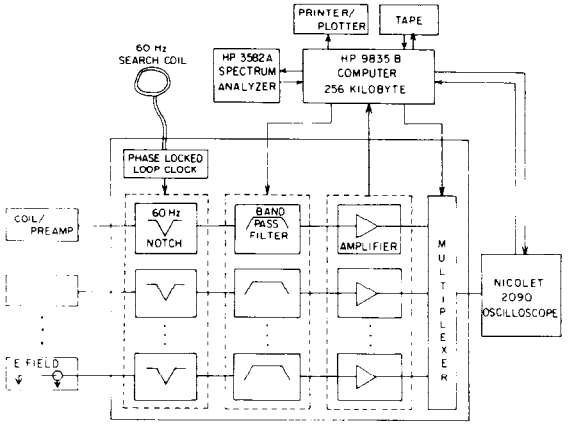

FIG. 8. Tipper-AMT data acquisition and processing system.

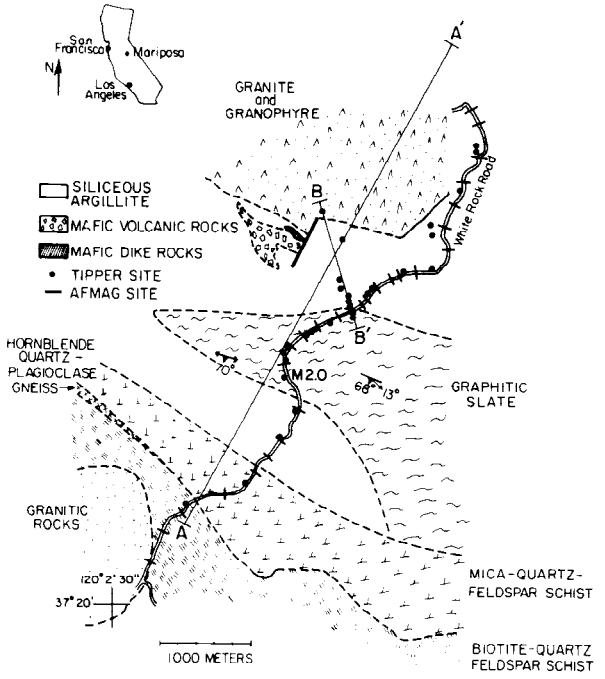

FIG. 9. Geology and station locations of Mariposa field site (after Best, 1963).

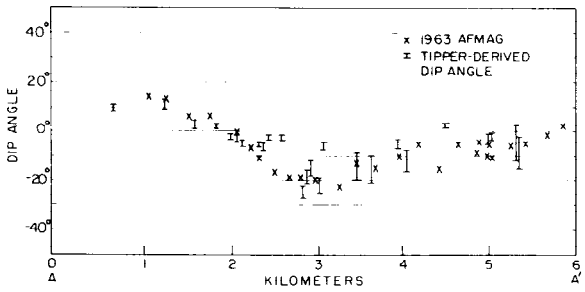

FIG. 10. Profile A-A' AFMAG and tipper-derived dip angles.

$$\langle n, n_r^* \rangle = 4kTR\Delta f, \tag{10}$$

where

k = Boltzmann's constant,
T = temperature (degrees K),
R = resistance (Ω),
Δf = observation bandwidth (Hz) and
$\langle n, n_r^* \rangle$ = noise power v^2.

SPICE models the operational amplifier noise (in our case the PMI OP-07) as the sum of resistive, current, and semiconductor voltage noises. It then computes the noise for each element and sums the entire circuit noise referenced to its output.

The cross-spectral noise levels determined in the field and the computer-modeled noise levels are in reasonably close agreement, as was the laboratory noise measurement. The agreement of these noise determinations implies that all the major noise sources have been taken into account. Figure 7 shows both the modeled and measured noise for the University of California coil design.

TIPPER DATA ACQUISITION SYSTEM

The data acquisition system designed for this experiment is capable of complete in-field processing of referenced tipper and magnetotelluric data in the audio- and subaudiofrequency ranges. The system is largely constructed from commercially available instrumentation in order to obtain maximum flexibility in the acquisition of experimental data and was not intended to fulfill the requirement of portability. It required very little design effort and has proven extremely capable and reliable. At the completion of this study when the equipment requirements were more firmly defined, we were able to implement a fully portable system weighing 55 kg (Labson et al., 1984).

As shown in Figure 8, the system consists of an analog signal conditioning segment, an analog 8 to 2 channel multiplexer, a two-channel Nicolet 2090 digital oscilloscope, a Hewlett-Packard 3582A Spectrum Analyzer, and a Hewlett-Packard 9835B computer. The analog portion of the system is powered by batteries, and the digital portion by a 120 Vac, 60 Hz motor generator. The analog instrumentation is composed of a power-line notch filter, band-pass filters, and amplifiers. The notch filter is a synchronous switched capacitor filter, phase locked to the power line frequency. It rejects the fundamental power line frequency and all its harmonics (Franks, 1973). Since all channels are locked to the power-line frequency, channel-to-channel drift is much less than in traditional notch filters. The notch filter has a useful passband of 1 to 500 Hz. For data acquisition outside this band, the filter is bypassed. The signal is band-pass limited by Ithaco 4212 four-pole Butterworth filters. High-pass filtering is used to preserve dynamic range, low-pass filtering is used for antialiasing. The eight filtered signals are multiplexed into the two input channels of the oscilloscope. Both the filters and the oscilloscope have selectable gain. Preamplifiers are included for very low-level signals. A frequency synthesizer provides the clocking signal for both the multiplexer and the oscilloscope's sample command. This clock is set to the frequency required for the band of interest. The oscilloscope holds the digital time series in its memory. Each signal's

time series has a 12 bit resolution and is 512 points long. The oscilloscope is controlled by the computer using the HPIB (IEEE-488) interface.

The program, written in Basic and assembly languages, consists of four parts: initialization, data acquisition, spectral averaging, and computation of results. The time series are obtained from the oscilloscope, Fourier transformed in the spectrum analyzer, and averaged as cross-power spectra in the computer. The cross-power spectra are then averaged again in windows with a constant bandwidth to center frequency ratio. Time series are typically obtained in blocks of 16. After obtaining each block, its averaged power spectrum is written to tape, and it is then averaged with the preceding blocks. The tipper and MT quantities and their confidence limits are computed from the running average.

This system implements several important features. The operator has the option of visually inspecting each time series before it is Fourier transformed and included in the cross-spectral average, thus allowing him to reject particularly noisy or saturated time series. This selection process greatly reduces the length of time required to achieve a given confidence interval. Tape recording power spectral averages as blocks resulting from a small number of time series allows further data editing and correction either in the field or at a later date. The system can be reconfigured in just a few minutes either as an MT receiver or a frequency-domain controlled-source receiver.

FIELD EXAMPLE

A demonstration field survey designed to show the utility and repeatability of the tipper measurement was conducted in the Sierra Nevada foothills near Mariposa, California during August and December, 1981, and February, 1982. The area is a geologically complex metamorphic terrain (Best, 1963) mapped in 1963 with AFMAG (Ward et al., 1966). The target, in plan view, is a wedge-shaped conductive graphitic slate surrounded by a resistive argillite (Figure 9), which produced a clear AFMAG anomaly when mapped in 1963 with AFMAG (Ward et al., 1966). An important aspect of our survey was a comparison of the AFMAG and tipper results.

The stations were acquired in pairs with 50 or 100 m separations. Each station consisted of three University of California induction coil magnetometers. The horizontal coils were buried in shallow trenches and oriented positive north and east. The vertical coil was partially buried in a hand-augered hole. Two orthogonal 30 m electric dipoles were placed at one of these stations. Thus every second station was also an MT measurement. Studies prior to this experiment had shown that for audio frequencies the measurement of the reference field could be made at from 1 to 500 m from the station with no discernible effect on the result. In processing the Mariposa data, it was found that identical results could be obtained from either a magnetic or electric field reference. Because the signal-to-noise ratio for the electric field measurements was much higher than the signal-to-noise ratio for the magnetic field, the electric field reference was used for all of the Mariposa tipper stations.

Thirty tipper stations were placed along the 1963 AFMAG profile. Several additional stations were located on a short profile perpendicular to the northern edge of the slate (Figure 9). The tipper was determined from 10 to 250 Hz at all sites with additional higher and lower bands as necessary. The natural field signal level was high in August and low in December and February. A minimum average of thirty-two 512 point time series was required for a measurement in August and a maximum of 192 in February corresponding to 0.5 and 2.5 hours, respectively. Averaging of time series continued at each site until the estimates of the parameters fell on a smooth curve.

Figure 10 shows the comparison of the 150 Hz, 1963 AFMAG and tipper-derived dip angles. The dip angle is the apparent tilt angle of the tipper's polarization ellipse at a given azimuth. For AFMAG the dip angle is defined by

$$\text{dip angle} = \tfrac{1}{2}\arctan\left[\frac{(2\cos(\phi)\,|\,T_\theta\,|)}{1-|\,T_\theta\,|^2}\right], \tag{11}$$

where T_θ is the ratio of vertical to horizontal magnetic field (H_z/H_θ) in the azimuthal θ direction and ϕ is the phase of H_z relative to H_θ. Similarly, a dip angle can be computed from the tipper for any azimuth by

$$\text{dip angle} = \tfrac{1}{2}\arctan\left[\frac{2\cos(\phi)\,|\cos(\theta)T_x + \sin(\theta)T_y|}{1-|\cos(\theta)T_x + \sin(\theta)T_y|^2}\right], \tag{12}$$

where T_x and T_y are the ratios of vertical magnetic field to horizontal field in the x- and y-directions as defined in equations (6) and (7), θ is the desired azimuth, and ϕ is the phase of H_z relative to $[\cos(\theta)H_x + \sin(0)H_y]$. For AFMAG measurements, the azimuth is selected as the direction of primary polarization of the horizontal magnetic field. Since the 1963 AFMAG azimuths were not known, the tipper dip angle's azimuth was selected to be N 10°E, which is a common summertime polarization direction at this location and which provided the best fit to the AFMAG result. The resultant tipper-derived dip angles are quite similar to the 1963 AFMAG dip angles. The quality of this correspondence was found to be very dependent upon the selected azimuth. Much of the scatter in both the AFMAG and the tipper-derived dip angles can be attributed to the great distances over which many of the points were projected to the profile.

At any one given site, the complex T_x and T_y components of the tipper tensor and a number of other useful parameters derived from these fundamental quantities can be presented as a function of frequency. This is done in Figure 11 for site M2.0 (Figure 9) which is located within the outcrop of the slate near its southern boundary. The data, acquired in August 1981, consist of sixty-four 512 point time series obtained in mid-afternoon. The cross-spectral estimates have been averaged into frequency windows with a constant center frequency to bandwidth ratio of 10. Each parameter is shown with its estimated 50 percent confidence interval (Gamble et al., 1979b). Contamination of the data by the 60 Hz power line is evident, most notably at 60, 180, and 480 Hz.

The five tipper quantities that are presented are

(1) tipper magnitude (Figure 11a),

$$|\underline{T}| = (|T_x|^2 + |T_y|^2)^{1/2}, \tag{13}$$

is a rotationally invariant ratio of the coherent vertical and horizontal magnetic fields.

(2) tipper dip direction (Figure 11b),

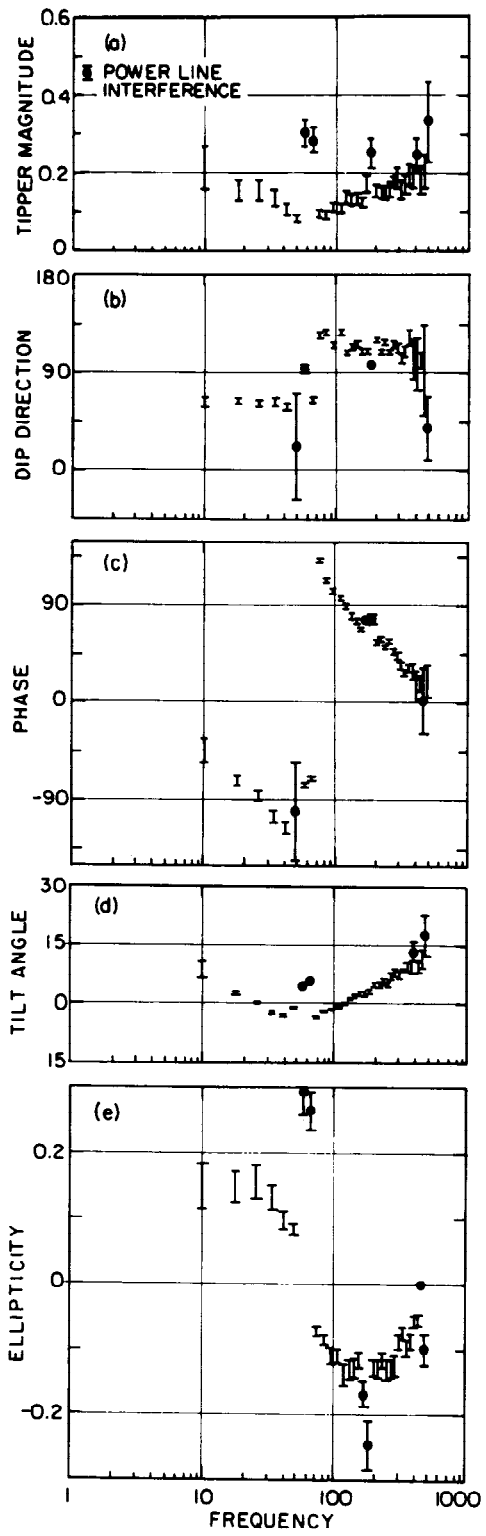

FIG. 11. Site M2.0 tipper functions: (a) tipper magnitude, (b) dip direction, (c) phase, (d) tilt angle, (e) ellipticity.

$$\theta = \tfrac{1}{2}\arctan\left[\frac{2[\mathrm{Re}\,(T_x)\,\mathrm{Re}\,(T_y) + \mathrm{Im}\,(T_x)\,\mathrm{Im}\,(T_y)]}{|T_x|^2 - |T_y|^2}\right], \tag{14}$$

is the direction of the horizontal magnetic field most highly coherent with the vertical magnetic field. This direction is perpendicular to the commonly used tipper strike direction. It is preferred over the strike direction because it may be interpreted to determine the direction to the conductor (Jupp and Vozoff, 1976).

(3) tipper phase (Figure 11c),

$$\phi = \arg\,[\cos\,(\theta)T_x + \sin\,(\theta)T_y], \tag{15}$$

is the phase of the tipper in the dip direction (i.e., phase of H_z with respect to H_θ).

(4) tilt angle (Figure 11d),

$$\psi = \tfrac{1}{2}\arctan\left\{\frac{2\ \mathrm{Re}\,[\cos\,(\theta)T_x + \sin\,(\theta)T_y]}{1 - |\cos\,(\theta)T_x + \sin\,(\theta)T_y|^2}\right\}, \tag{16}$$

is the tilt of the magnetic field's polarization ellipse in the dip direction (Born and Wolf, 1980, chap. 10).

(5) ellipticity (Figure 11e),

$$\varepsilon = \tan\left(\tfrac{1}{2}\arcsin\left\{\frac{-2\ \mathrm{Im}\,[\cos\,(\theta)T_x + \sin\,(\theta)T_y]}{1 + |\cos\,(\theta)T_x + \sin\,(\theta)T_y|^2}\right\}\right) \tag{17}$$

is the ellipticity of the magnetic field's polarization ellipse in the dip direction. These quantities are computed in the field with their associated confidence limits.

A possible explanation of the site M2.0 tipper is that the tipper is responding to two electrical conductivity anomalies. The minimum seen in the tipper at about 70 Hz marks the separation of these anomalies. The dip direction of the low-frequency anomaly is consistent with the southern boundary of the slate, and the dip direction of the high-frequency anomaly is consistent with the northern edge. This site is complicated by numerous small faults in the vicinity, some of which seem to be parallel to the northern edge of the slate. It is possible that the high-frequency anomaly is due to one of these faults rather than to the northern edge of the slate. This separation of anomalies is an important characteristic of the use of a broad range of frequencies. This is in contrast to the AFMAG result where little difference could be seen in the 150 and 500 Hz measurements (Ward et al., 1966). Had AFMAG been capable of measuring at other frequencies, in this case 20 Hz, a different conclusion as to its frequency sensitivity might have been reached.

For the tipper to offer any advantage over AFMAG, the result must be repeatable at any time of the year. Site M2.0 was reoccupied several times in August, 1981 as well as in December, 1981 and February, 1982. Figure 12 shows the polarization ellipse of the vertical-to-horizontal magnetic field in the dip direction with values of several other tipper functions. Low-frequency data were acquired five times, high-frequency data three times. There is no significant difference seen within either the 18–23 Hz or 130–150 Hz frequency bands, even though the

natural field's polarization and spectral amplitude varied widely from one time to the next.

Examination of the tipper quantities introduced in equations (13) through (17) along the 1963 AFMAG profile demonstrates the effectiveness of the tensor measurement. The 150 Hz profile shows that the tipper may be used to outline the body, as well as to indicate its geometry. Much of the scatter is again due to projection to the profile.

The tipper (Figure 13a) is asymmetric, with a small peak at the southern boundary of the slate and a much larger peak at the northern boundary. Examination of the slate-argillite contact shows that to the south the rocks are an alternating sequence of argillite and slate approximately 100 m wide, whereas the northern contact is abrupt. The large tipper values correspond to the abrupt northern contact. The tipper phase (Figure 13b) changes by 180 degrees crossing the slate, as would be expected when a conductor is crossed. The tilt angle (Figure 13c) is similar to the tipper with a small positive peak to the south and a larger negative peak to the north. The magnitude of the tilt angle is generally larger than the magnitude of the 150 Hz AFMAG dip angle. The ellipticity (Figure 13d) shows large negative values over the slate. A three-dimensional effect is seen in the tipper dip direction (Figure 13e) where the direction shifts by approximately 90 degrees from -135 degrees in the south to 135 degrees in the north. These directions are roughly perpendicular to the mapped outline of the slate. This geometric information is an important feature of the tensor tipper measurement, because the wedge shape of the conductor can, at least in part, be inferred from a single profile.

The ability of the tipper to map irregular bodies is more clearly seen by examining the tipper in plan view as shown in Figure 14. To produce the plan view, the tipper is rotated through 360 degrees such that

$$|\underline{T}| = |\cos(\theta)T_x + \sin(\theta)T_y| \tag{18}$$

where $\theta = 0$ to 360 degrees.

The tippers at 18–23 Hz and 130–150 Hz are quite similar. At both frequencies the major axis of the rotational figure is generally perpendicular to the conductor, becoming clearer at 130–150 Hz which is nearer the peak response at most sites. In the case of a 2-D body, the minor axis of the rotated tipper is zero since there is no tipper component in the body's strike direction. The minor axis is large at 18–23 Hz, implying a 3-D effect.

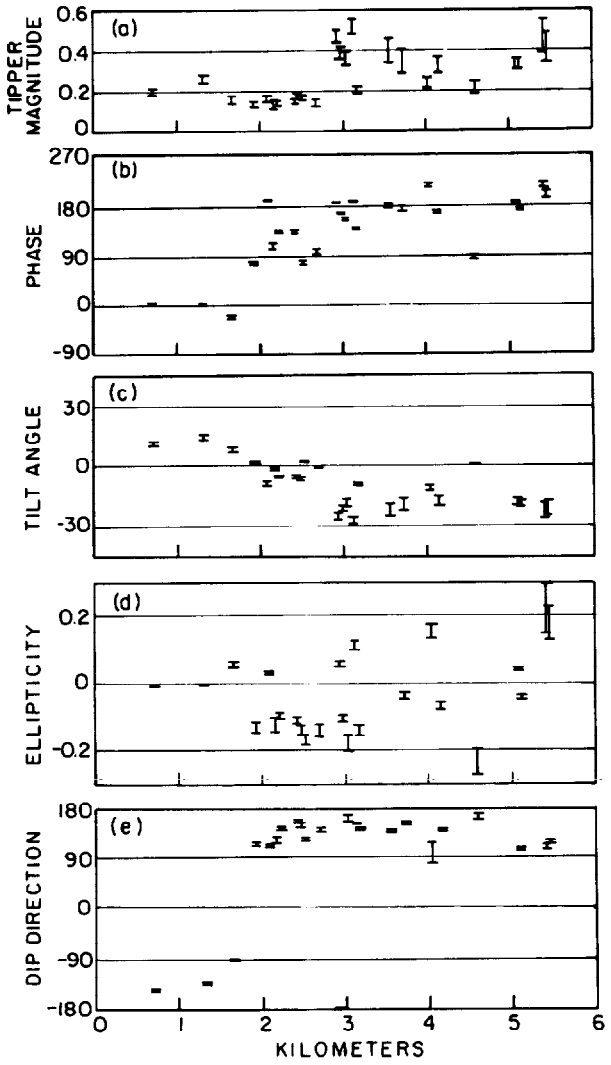

FIG. 13. Profile A-A' tipper functions, 130–150 Hz: (a) tipper magnitude, (b) phase, (c) tilt angle, (d) ellipticity, (e) dip direction.

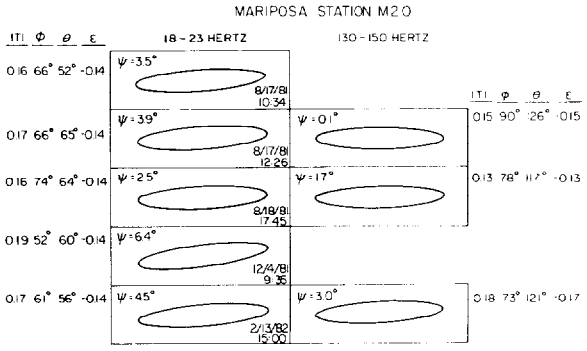

FIG. 12. Repeatability of tipper at station M2.0 in 18–23 Hz and 130–150 Hz bands: $|\underline{T}|$, tipper magnitude; ϕ, tipper phase; θ, dip direction; ψ, tilt angle; ε, ellipticity.

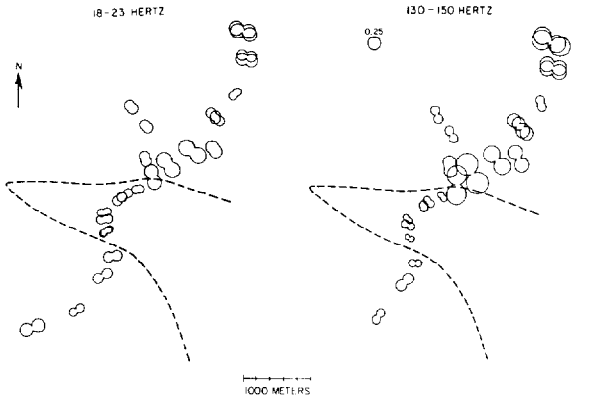

FIG. 14. Plan view of rotated tipper values for Mariposa field site with outline of graphitic slate in 18–23 Hz and 130–150 Hz bands.

This effect is much less pronounced at 130–150 Hz. In spite of the obvious three-dimensionality of the body, the tipper outlines it quite well with small tipper values identifying sites within the conductor.

CONCLUSION

The Mariposa study demonstrates that the tipper obtained from natural audiofrequency magnetic fields can be used for mapping a complex conductive target. As an improvement over AFMAG, the tipper is repeatable on a year-round basis and is independent of the polarization state of the natural source field. The use of the MT remote reference technique for tipper measurements makes it possible to obtain high-quality data using easily portable sensors, even during periods of low signal level. The use of a broad band of frequencies aids distinguishing features of different electrical conductivity. Our ability to exploit a great range of frequencies makes this method attractive for use in areas where depths of exploration may range from several meters to several kilometers.

ACKNOWLEDGMENTS

We wish to thank F. C. Frischknecht, D. B. Hoover, and C. L. Tippens of the U.S.G.S. for assistance with the section concerning the U.S.G.S. AMT coil. This work was supported by the Branch of Geophysics, U.S. Geological Survey, Denver, CO and by the Earth Science Division, Lawrence Berkeley Laboratory, Berkeley, CA.

REFERENCES

Anav, A., Cantarano, S., Cerruli-Irelli, P., and Pallotino, G. V., 1976, A correlation method for measurement of variable magnetic fields: Inst. Elect. and Electron. Eng. Trans., Geosc. Elect., **GE14**, 106–114.

Bendat, J. S., and Piersol, A. G., 1971, Random data: analysis and measurement procedures: Wiley-Interscience.

Best, M. G., 1963, Petrology and structural analysis of metamorphic rocks in the southwestern Sierra Nevada foothills, California: Univ. of Calif. Publ. Geol. Sci., **42**, 111–158.

Born, M., and Wolf, E., 1980, Principles of optics, 6th ed.: Pergamon Press, Inc.

Bostick, F. X., Jr., Smith, H. W., and Boehl, J. E., 1977, Magnetotelluric and dc dipole-dipole soundings in northern Wisconsin: Final Tech. Rep., Elect. Eng. Res. Lab., Univ. of Texas, Austin.

Franks, L. E., 1973, *N*-path filters, *in* Modern filter theory and design: Temes and Mitra, Eds., John Wiley and Sons, Inc.

Gamble, T. D., Goubau, W. M., and Clarke, J., 1979a, Magnetotellurics with a remote reference: Geophysics, **44**, 53–68.

——— 1979b, Error analysis for remote reference magnetotellurics: Geophysics, **44**, 959–968.

Hoover, D. B., Long, C. L., and Senterfit, R. M., 1978, Some results from audio magnetotelluric investigations in geothermal areas: Geophysics, **43**, 1501–1514.

Jupp, D. L. B., and Vozoff, K., 1976, Discussion on "The magnetotelluric method in the exploration of sedimentary basins": Geophysics, **41**, 325–328.

Labson, V. F., Frischknecht, F. C., and Becker, A., 1984, A portable tensor magnetotelluric receiver design and field test: Presented at the 54th Annual International SEG Meeting, December, Atlanta.

Macintyre, S. A., 1980, A portable low noise low frequency search coil magnetometer: Inst. Elect. and Electron. Eng., Trans. Mag. V. Mag-16, 5.

Maxwell, E. L., and Stone, D. L., 1963, Natural noise fields from 1 C/S to 100 KC/S: Office of Naval Research, rep. no. NR371-590, Washington, D.C.

Schmucker, U., 1970, Anomalies of geomagnetic variations in the southwestern United States: Bull., Scripps Inst. Ocean., Univ. of Calif. San Diego, **13**.

Strangway, D. E., Swift, C. M., Jr., and Holmer, R. C., 1973, The application of audio-frequency magnetotellurics (AMT) to mineral exploration: Geophysics, **38**, 1159–1175.

Telford, W. M., 1977, Characteristics of audio and sub-audio telluric signals: Geophys. Prosp., **25**, 321–333.

Vladimirescu, A., Zhang, K., Newton, A. R., Pederson, P. O., Sangiovani-Vincentelli A., 1981, SPICE version 2G users guide: Dept. of Elect. Engin. and Comp. Sci., Univ. of California, Berkeley.

Vozoff, K., 1972, The magnetotelluric method in the exploration of sedimentary basins: Geophysics, **37**, 98–141.

Ward, S. H., 1959, AFMAG—airborne and ground: Geophysics, **24**, 761–789.

Ward, S. H., O'Donnell, J., Rivera, R., Ware, G. H., and Fraser, D. C., 1966, AFMAG—applications and limitations: Geophysics, **31**, 576–605.